ACS Catalysis

pubs.acs.org/acscatalysis

Research Article

Alcohol-Induced Low-Temperature Blockage of Supported-Metal Catalysts for Enhanced Catalysis

Felipe Polo-Garzon,* Thomas F. Blum, Victor Fung, Zhenghong Bao, Hao Chen, Zhennan Huang, Shannon M. Mahurin, Sheng Dai, Miaofang Chi, and Zili Wu*

Cite This: *ACS Catal.* 2020, 10, 8515–8523

Read Online

ACCESS | Metrics & More | Article Recommendations | Supporting Information

ABSTRACT: The partial or complete blockage of active sites of metal nanoparticles (NPs) on supported-metal catalysts has been of interest for tuning the stability, selectivity, and rate of reactions. Here, we show that Au-sites in Au/TiO_2 surprisingly become blocked upon treatment in common alcohols (2-propanol and methanol), with 2-propanol causing a greater extent of blockage. Nearly 95% of Au-sites are covered after treatment in 2-propanol at room temperature, followed by desorption at 150 °C. Infrared spectroscopy of CO adsorption unambiguously confirms the occurrence of this phenomenon. Electron energy loss spectroscopy (EELS), temperature-programmed desorption (TPD), Raman spectroscopy, and DFT simulations suggest that the formation of carbon deposits from 2-propanol decomposition and/or the migration of a TiO_x layer over the supported NPs may be responsible for the blockage of Au-sites. Nearly full coverage of Au NPs after treatment in 2-propanol led to negligible activity for catalytic CO oxidation, whereas partial retraction of the overlayer led to enhanced activity with time-on-stream, suggesting a self-activating catalytic performance.

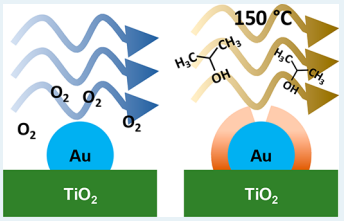

KEYWORDS: *carbon deposition, strong metal–support interaction, gold catalysis, FTIR, EELS, CO oxidation*

INTRODUCTION

Supported Au nanocatalysts present intriguing properties, and their outstanding performances have made them suitable for industrial applications.[1] However, the deactivation of Au nanocatalysts under reaction conditions has been reported for various systems, including conversion of alcohols, CO oxidation, and propene epoxidation.[2−7] Strong metal−support interactions (SMSIs), which consist of the migration of the oxide support over the supported NPs,[8−15] have been used as one of the tools to enhance catalyst stability.[4,16−18]

Promoting SMSI on supported Pt and Pd NPs has shown to be more favorable than for Au,[19] because Au presents a low work function and surface energy.[19−21] However, Tang et al. have shown that it is indeed possible to induce SMSIs for supported Au NPs.[4,16−18] In their work, the extent of coverage of Au NPs in Au/TiO_2 during "classical" SMSI treatment (H_2 treatment at high temperatures (>400 °C)) is dependent on the synthesis procedure and the crystallographic phase of the TiO_2 support. In fact, some samples did not achieve full coverage of Au NPs after H_2 treatment up to 600 °C. Anatase was reported as the crystallographic phase of TiO_2 most susceptible to SMSI upon treatment in H_2, followed by 80% anatase+20% rutile, and with pure rutile as the least susceptible.[4] This intriguing behavior led us to explore if there are alternate ways to induce coverage of Au NPs due to SMSI in Au-samples that do not favor SMSI under H_2. The catalyst sample under study herein is a Au/TiO_2 sample (80% anatase, 20% rutile) that did not present SMSI under H_2 treatment at 600 °C (Figure S1). This sample is commercially available and thus accessible to many research laboratories, therefore, the findings reported herein are directly relevant to a broad audience.

Since reduction of Au/TiO_2 in H_2 has led to SMSI[4] and alcohols have been shown to promote the reduction of metal oxides,[22,23] even below 100 °C on TiO_2,[24] we hypothesized that alcohol-induced reduction of the catalyst could result in SMSI at lower temperatures than with H_2. The inherent challenge while testing this hypothesis is that alcohol dissociation on the surface may lead to carbonaceous species that cover the Au NPs, which may mislead the conclusions about the migration of the TiO_x layer from the support. Blockage of catalytic sites through the deposition of strongly bound adsorbates has been vastly reported.[25] Recently, it was shown that 2-propanol conversion over $Pd/Au/TiO_2$ leads to catalyst deactivation at low temperature (75 °C), without deactivation at moderate temperature (125 °C). Such deactivation was attributed to strong binding of intermediates to surface active sites.[2]

Herein, carefully performed spectroscopy experiments show that treatment of Au/TiO_2 with common alcohols (2-propanol and methanol) near room temperature (followed by

Received: June 3, 2020
Revised: June 29, 2020
Published: July 20, 2020

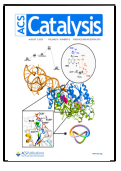

desorption at 150−300 °C) indeed induces blockage of Au-sites. 2-Propanol showed a greater extent of coverage of Au NPs, and thus, it became the focus of the present study. After Au/TiO_2 was treated in 2-propanol, oxygen treatment at temperatures higher than ∼230 °C retracts the overlayer blocking the Au-sites. Partial retraction of the overlayer changes the nature of the active sites on Au/TiO_2 for CO oxidation, making the catalyst resistant to deactivation over time. Our study suggests that blockage of Au-sites is a consequence of SMSI and/or carbon deposits. In any case, it is remarkable that near-*full* coverage of Au-sites can be induced by exposing the sample to 2-propanol at room temperature (followed by desorption at 150 °C) and that such coverage persists even up to 200 °C when the sample is exposed to O_2. In addition, it is remarkable that partial retraction of the blocking overlayer leads to enhanced catalysis for CO oxidation.

EXPERIMENTAL SECTION

Catalysts. Au/TiO_2 (1 wt % Au, Au particle size ∼3 nm, BET surface area = 47.5 m^2/g) was obtained from the World Gold Council.[26,27]

Au/SiO_2 (1.9 wt %, Au particle size of ∼6−7 nm, Figure S2a) was synthesized using the precursor $Au(en)_2Cl_3$ (en= ethylenediamine).[28] A brief description is presented as follows. First, the precursor $Au(en)_2Cl_3$ was synthesized by mixing ethylenediamine (0.45 mL), $HAuCl_2{\cdot}3H_2O$ (1 g), and H_2O (10 mL) to form a transparent brown solution. Addition of ethanol (70 mL) produced a precipitate that was filtered, washed with ethanol, and dried overnight in a vacuum oven at 40 °C. Second, the precursor is adsorbed on SBA-15. $Au(en)_2Cl_3$ (0.372 g) was dissolved in H_2O (150 mL). The pH of the solution was adjusted to 10 by addition of a NaOH solution (5.0 wt %). Next, 2 g of SBA-15 was added. The pH value of the solution decreased immediately, and the final pH value was controlled between 6 and 10 by the further addition of the NaOH solution. The mixed solution was stirred for an additional 2 h. The final product was dried in a vacuum oven for 2 days. The yellowish product was then reduced by flowing 4% H_2/Ar at 150 °C for 1 h. Calcination in O_2 at 450 °C was performed to remove ligands covering the Au NPs.

Au/CeO_2 (5.0 wt % Au, Au particle size of ∼5 nm, BET surface area = 36.6 m^2/g, Figure S2b) was synthesized by preparing the CeO_2 first and then supporting the Au NPs. The CeO_2 polyhedra were prepared using a previously reported hydrothermal method.[29] Briefly, in a typical synthesis, 0.868 g of $Ce(NO_3)_3{\cdot}6H_2O$ and 16 mg of NaOH were dissolved in 5 and 35 mL of deionized water. The two solutions were mixed and transferred to a 125 mL autoclave with a Teflon liner. The autoclave was then heated to 373 K and kept for 24 h. After the hydrothermal synthesis, the as-synthesized ceria was washed in deionized water and ethanol at room temperature and then dried at 90 °C overnight in air. To deposit the Au NPs, 0.5 g of CeO_2, 55 mg of $HAuCl_3$, 1.28 g of urea, and 60 mL of H_2O were mixed together to form a suspension. The suspension was stirred and kept at 80 °C in an oil bath for ∼20 h. The end product was washed, collected, and annealed in air at 300 °C for 3 h.

Inductively Coupled Plasma Atomic Emission Spectroscopy (ICP-AES). ICP-AES was performed by Galbraith Laboratories, INC.

BET Surface Area. A Micromeritics Gemini VII Surface Area and Porosity Analyzer was used to perform Nitrogen physisorption at −196 °C. The surface areas were calculated using the BET method.[30]

X-ray Diffraction (XRD) Patterns. XRD patterns were collected with a PANalytical Empyrean system using Cu Kα radiation. Diffractograms were obtained at incident angles for 2θ = 5−90°.

FTIR Spectroscopy of CO Adsorption. Experiments were performed at atmospheric pressure using a Thermo Nicolet Nexus 670 FTIR spectrometer with an MCT detector. Each spectrum was recorded with 32 scans at a resolution of 4 cm^{-1}. The sample was loaded into a porous ceramic cup, and the cup was inserted into a Diffuse Reflectance Infrared Fourier Transform Spectroscopy (DRIFTS) cell (Pike Technologies). The sample was activated in a diffuse reflectance cell (Pike Technologies) at different temperatures and under different gases for 30 min, before the gas flow was switched to 30 mL/min of Ar, and background spectra were taken at 30 °C (or −150 °C). After a background spectrum was collected, 30 mL/min of 1%CO/(Ar+He) was flowed through the catalyst for 10 min, followed by desorption for 10 min (CO adsorption was done at 30 or −143 ± 2 °C). The catalysts were pretreated under 30 mL/min of 3% O_2/Ar or under 30 mL/min of 6% 2-propanol/Ar (using a saturator filled with liquid 2-propanol at 25 °C), unless otherwise noted. After the catalyst was treated in O_2 or 2-propanol, it was flushed in Ar for 10 and 30 min at 300 °C, respectively. For instance, for data reported in Figure 1a, the explicit procedure was the following:

Spectrum "$O_2$300 °C"

1. Treat in O_2/Ar at 300 °C for 30 min.
2. Flush catalyst with Ar at 300 °C for 10 min.
3. Cool down to 30 °C in Ar. Collect background spectrum at 30 °C.
4. Collect spectra of CO adsorption for 10 min.
5. Collect spectra of CO desorption (in Ar) for 10 min.

Spectrum "2-propanol 30 °C"

6. Desorb CO by flushing O_2/Ar at 300 °C for 30 min.
7. Flush catalyst with Ar at 300 °C for 10 min.
8. Cool to 30 °C in Ar.
9. Treat in 2-propanol/Ar at 30 °C.
10. Desorb 2-propanol in Ar at 30 °C for 30 min.
11. Desorb 2-propanol in Ar at 300 °C for 30 min.
12. Cool to 30 °C in Ar. Collect background spectrum at 30 °C.
13. Collect spectra of CO adsorption for 10 min.
14. Collect spectra of CO desorption (in Ar) for 10 min.
15. **Spectrum "2.8 days in $O_2$30 °C"**
16. Flow O_2/Ar through catalyst for 2.8 days at 30 °C.
17. Desorb CO in Ar at 300 °C for 30 min.
18. Cool to 30 °C in Ar. Collect background spectrum at 30 °C.
19. Collect spectra of CO adsorption for 10 min.
20. Collect spectra of CO desorption (in Ar) for 10 min.

Temperature-Programmed Desorption (TPD). TPD experiments were performed in an Altamira Instruments system (AMI-200). The catalyst sample was loaded into a U-tube quartz reactor. Before TPD experiments from 30 to 920 °C, the sample was treated in 45 mL/min of 8% O_2/Ar or in 6% 2-propanol/Ar (45 mL/min Ar bubbled through a saturator). The ramping rate was 10 °C/min. The outlet from the reactor was analyzed using an OmniStar mass spectrometer from Pfeiffer Vacuum. The masses followed were 28 (CO), 41 (propene), 44 (CO_2), 45 (2-propanol), and 58

https://dx.doi.org/10.1021/acscatal.0c02452
ACS Catal. 2020, 10, 8515−8523

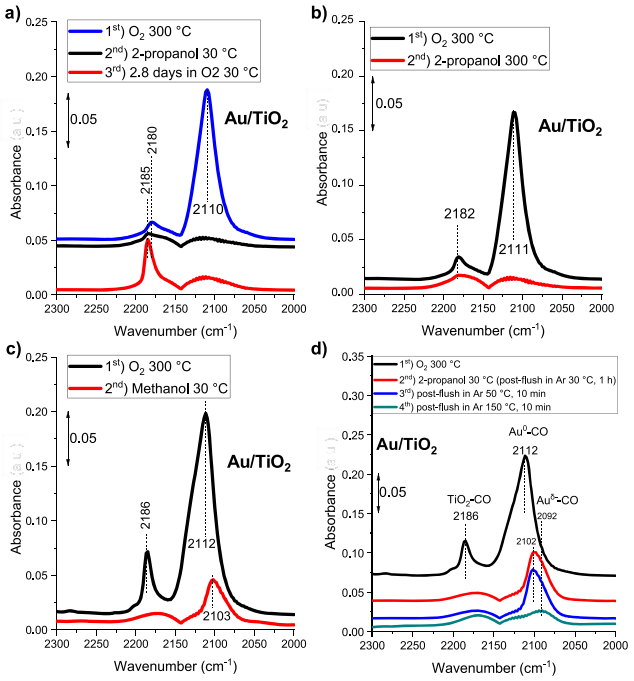

Figure 1. FTIR spectroscopy of CO adsorption (after 10 min) at 30 °C on Au/TiO_2 (a) after treatment in O_2 at 300 °C, treatment in 2-propanol at 30 °C (with postflush in Ar at 300 °C), and after exposure to O_2 for 2.8 days at 30 °C; (b) after treatment in O_2 at 300 °C and treatment in 2-propanol at 300 °C (with postflush in Ar at 300 °C); (c) after treatment in O_2 at 300 °C and treatment in methanol at 30 °C (with postflush in Ar at 300 °C); (d) after treatment in O_2 at 300 °C, after treatment in 2-propanol at 30 °C, and after postflush in Ar at 50 and 150 °C (2^{nd}, 3^{rd}, and 4^{th} share the same background). Note: "1^{st}", "2^{nd}" and "3^{rd}" represent the sequence in the collection of spectra. Each "set" of spectra (there are four sets: panels a, b, c, and d) was collected for a fresh load of the Au/TiO_2 catalyst in the DRIFTS cell.

(acetone). The contributions from different components to a single mass were decoupled and subtracted.

Microscopy. Au/TiO_2 was treated in 2-propanol at 300 °C *ex situ*, then, images were collected in a NION UltraSTEM 100 kV microscope and electron energy loss spectroscopy (EELS) analysis was performed. The normalized signal intensity versus line scan coordinate was generated by subtracting the background from each EELS edge, then integrating the signal, and finally dividing by the scattering cross section for the given window of integration. *In situ* thermal treatment of the sample was not performed before imaging. The line scan was taken at room temperature with a 100 kV electron beam.

Au/SiO_2 and Au/CeO_2 were dispersed onto 200-mesh copper grids with a lacey carbon support by immersion of the grids into the dry powder. Scanning transmission electron microscopy (STEM) was carried out on a Hitachi HD-2000 ultrathin film evaluation system with a 200 kV accelerating voltage.

Raman Spectroscopy. *In situ* Raman spectroscopy was performed on a multiwavelength Raman system[31] at room temperature and at 300 °C using 442 nm visible laser excitation. Raman scattering was collected via a customized ellipsoidal mirror and directed by a fiber optics bundle to the spectrograph stage of a triple Raman spectrometer (Princeton InstrumentsActon Trivista 555). Edge filters (Semrock) were used in front of the UV−vis fiber optic bundle (Princeton Instruments) to block the laser irradiation. The 442 nm (10 mW at sample) excitation is generated from a HeCd laser (Melles Griot). A UV-enhanced liquid N_2-cooled CCD detector (Princeton Instrument) was employed for signal detection. The procedure for data collection was as follows: (1) 10 mg of Au/TiO_2 was loaded into the Raman cell, and one measurement was collected at room temperature without any pretreatment. (2) The temperature was increased to 300 °C while flowing 30 mL/min of 5% O_2/Ar, and the temperature was held at 300 °C for 30 min while flowing O_2/Ar; next, the system was flushed with 30 mL/min of Ar for 10 min, and a spectrum was collected. (3) 30 mL/min of Ar was saturated with 2-propanol using a bubbler, and the mixture was flowed over Au/TiO_2 for 30 min (still at 300 °C), then a spectrum was collected. (4) The flow was switched back to 30 mL/min of Ar while still holding the temperature at 300 °C for 30 min, then a spectrum was collected. (5) Finally, 30 mL/min of 5% O_2/Ar was flowed over the catalyst for 30 min at 300 °C, and a spectrum was collected.

To test whether the observed carbon deposition was caused by the laser during step 3, a control experiment was performed in which steps 1−3 were performed without exposing the sample to the laser, and only at the end of step 4 was the sample exposed to the laser for collection of a spectrum. It was concluded that carbon deposition was not due to exposure to the laser.

DFT Calculations. All periodic density functional theory (DFT) calculations were performed with the Vienna ab initio Simulation Package (VASP).[32,33] The Perdew−Burke−Ernzerhof (PBE)[34] functional of generalized-gradient approximation (GGA) was used for electron exchange and correlation. The electron−core interaction was described using the projector-augmented wave method (PAW).[35,36] A force convergence of 0.05 eV/ Å was used. All calculations were performed with spin polarization. For all models, a vacuum layer of 15 Å was used to prevent interactions between the periodic cells, and the bottom two layers were fixed during optimization. To model the covered Au surface from SMSI, a monolayer of Ti_2O_3 (001) in a 2 × 2 cell was placed on the Au (111) $\sqrt{3} \times \sqrt{3}$ surface to simulate a reduced titanium oxide layer.

The free energy of formation (ΔG) of the SMSI structure was calculated according to the formula:

$$\Delta G = \frac{1}{A}(E_{Ti_xO_y/Au} - E_{Au} - E_{TiO_{2,bulk}} \cdot x - E_{O_2} \cdot (y - 2x) - \Delta\mu_{O_2} \cdot (y - 2x))$$

where $E_{Ti_xO_y/Au}$ is the energy of the Ti_xO_y layer deposited on the Au slab, E_{Au} is the energy of the Au slab, $E_{TiO_{2,bulk}}$ is the energy of bulk TiO_2, E_{O_2} is the energy of gas-phase oxygen, $\Delta\mu_{O_2}$ is the change in oxygen chemical potential, and A is the area of the surface generated.

Kinetic Measurements. The catalytic oxidation of carbon monoxide at 50 °C and near-atmospheric pressure was performed in an Altamira Instruments system (AMI-200). Each catalyst sample (2−42 mg, sieved to 177−250 μm) was diluted with quartz sand (177−250 μm) and loaded into a U-tube quartz wool. The quartz-to-catalyst mass ratio was approximately 6:1. The partial coverage of Au NPs due to partial retraction of the blocking overlayer exposes fewer catalytic sites than the base sample without treatment in 2-propanol, and thus, to compare the catalysts at similar

https://dx.doi.org/10.1021/acscatal.0c02452
ACS Catal. 2020, 10, 8515−8523

conversions, different amounts of catalyst were loaded in the reactor. When the sample without treatment in 2-propanol was tested using 42 mg, the conversion of CO to CO_2 was 100% (Figure S3), which does not allow studying the deactivation process. Therefore, the amount of catalyst loaded to the reactor was reduced to 2.2 mg in this case. The total flow of gas entering the reactor was 50 mL/min, consisting of 0.8% CO, 1% O_2 and balance Ar+He. Each sample was pretreated *in situ* under 45 mL/min of 8% O_2/Ar and/or 45 mL/min saturated with 2-propanol (45 mL/min of 6% 2-propanol/Ar) as described in the main text. Products were analyzed using a Buck Scientific Model 910 gas chromatograph (GC) equipped with a flame ionization detector and a HayeSep-D column.

RESULTS AND DISCUSSION

Infrared (IR) spectroscopy of CO adsorption is a commonly used technique to probe the availability of metal sites, as the adsorption of CO on exposed Au presents very distinct vibrational modes. Au/TiO_2 was treated *in situ* under O_2 at 300 °C, and a spectrum during CO flow at room temperature was collected (Figure 1a–d). The vibrational mode at 2110–2112 cm^{-1} is characteristic of CO adsorption on metallic (or slightly cationic) Au.[3] A subsequent treatment in 2-propanol at 30 °C, followed by a desorption in Ar at 300 °C (temperature needed to desorb 2-propanol, and its decomposition products: acetone, propene), completely prevented the adsorption of CO on Au, suggesting the blockage of Au-sites upon treatment in 2-propanol. The overlayer covering Au-sites showed to be stable upon oxygen exposure for ~3 days at 30 °C (Figure 1a). The band at 2180–2186 cm^{-1} is attributed to CO adsorption on coordination unsaturated Ti sites on TiO_2.[37,38] Treatment in 2-propanol at 300 °C also prevented the adsorption of CO (Figure 1b). The particle size of the Au NPs did not change during O_2, CO, or 2-propanol treatment at 300 °C (~3 nm, see Figure S4); thus, the decrease in CO adsorption is not due to sintering of Au NPs upon treatment. Treatment of the sample in methanol at 30 °C followed by a desorption at 300 °C showed drastic reduction of CO adsorption on Au sites (Figure 1c), although blockage of Au sites was not as extensive as with the treatment in 2-propanol at 30 °C (Figure 1a). Hereafter, we focus on the blockage of Au-sites after treatment in 2-propanol.

IR spectroscopy results showed full coverage of Au NPs after treatment in 2-propanol at 30 °C and Ar-flush at 300 °C (Figure 1a). To elucidate whether the blockage of Au sites occurs during the exposure to 2-propanol at 30 °C or during the desorption process of 2-propanol at temperatures between 30 and 300 °C where different products can be formed from 2-propanol conversion and desorbed from the surface (see Figure 2a), further experiments were performed (Figure 1d). Au/TiO_2 was exposed to 2-propanol at 30 °C for 30 min and then flushed in Ar at 30 °C for 1 h, showing a significant reduction in the number of Au-sites available for CO adsorption; however, these sites were not fully covered. Upon desorption of the species associated with 2-propanol adsorption/decomposition at 150 °C, more than 95% of the Au sites were covered. This confirms full coverage of Au-sites after exposure to 2-propanol at 30 °C is only achieved when the temperature of the system is increased beyond 150 °C when the desorption chemistry-induced transformation of the catalyst surface can fully occur. In Figure 1, the relative intensity of peaks at 2180–2186, 2110–2112, and the shoulder at 2130 cm^{-1} after O_2 treatment at 300 °C slightly changes

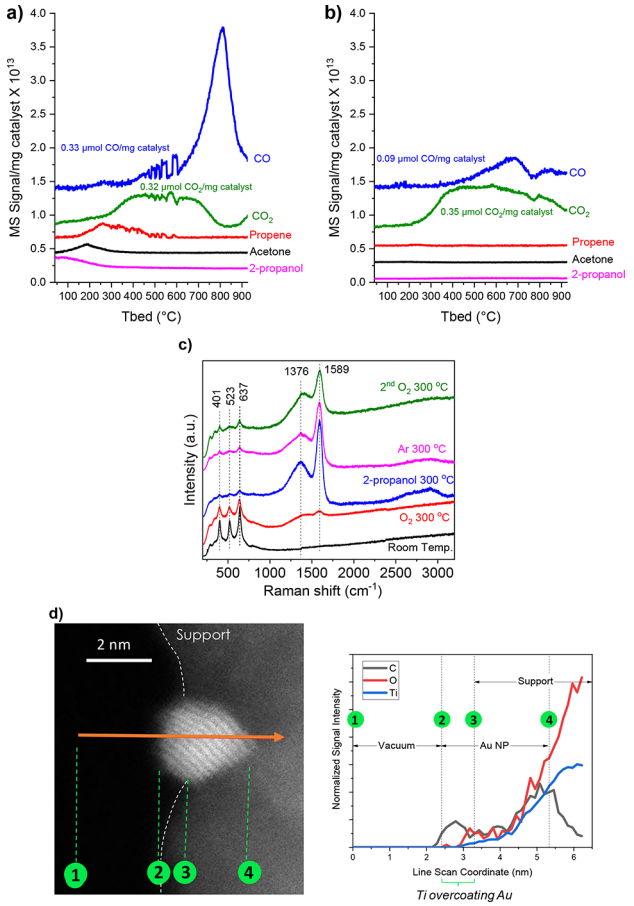

Figure 2. Characterization of Au/TiO_2. (a) TPD after 2-propanol treatment at 30 °C. (b) TPD after O_2 treatment at 300 °C. (c) Raman spectroscopy under different atmospheres. (d) STEM and EELS analysis of Au/TiO_2 after 2-propanol treatment at 300 °C. Line scan follows orange arrow on the image to the left.

because minimal changes (±3 min) in the duration of the O_2 treatment at 300 °C impact the traces of desorbed species in the DRIFTS cell (Figure S5), covering slightly less/more surface sites. Despite these small differences, the suppresion of CO adsorption on Au sites upon treatment with 2-propanol and methanol is evident.

IR spectroscopy was also utilized to characterize the species on the surface after CO adsorption (Figure S6a), 2-propanol desorption (Figure S6b), and methanol desorption (Figure S6c) on Au/TiO_2. CO_2 was formed upon exposure of Au/TiO_2 to CO at 30 °C through the interaction with surface oxygen. A variety of carbonate species were observed (Figure S6a). After adsorbing 2-propanol at 30 °C and desorbing it in Ar at 300 °C, surface 2-propoxy, acetate and carbonate species are observed (Figure S6b). After adsorbing methanol at 30 °C and desorbing it in Ar at 300 °C, surface methoxy and formate species remain on the surface (Figure S6c) (see details in Supporting Information). Therefore, although flushing the Au/TiO_2 sample with Ar at 300 °C fully desorbs gas-phase 2-propanol, acetone, and propene (see TPD results next), adsorbed carbonaceous species remain on the surface.

Temperature-programmed desorption (TPD) results confirm that the treatment in 2-propanol leaves additional carbonaceous species on the surface (Figure 2a), when compared with the sample before 2-propanol treatment (Figure 2b). As observed in Figure 2a, although unreacted 2-

https://dx.doi.org/10.1021/acscatal.0c02452
ACS Catal. 2020, 10, 8515–8523

propanol and the dehydration/dehydrogenation products (propene/acetone) desorb at temperatures below 300 °C, tightly bound species with desorption temperatures as high as 800 °C remain on the surface. The buildup of carbon deposits after treatment in 2-propanol at 300 °C was additionally characterized using *in situ* Raman spectroscopy (Figure 2c) in order to unveil whether the treatment in 2-propanol induced changes in the TiO_2 structure. Raman shifts at 1376 and 1589 cm^{-1} reveal the creation of carbon deposits upon treatment in 2-propanol. Characteristic Raman bands of TiO_2 anatase (the Au/TiO_2 sample under study is 80% anatase) are evident at 401, 523, and 637 cm^{-1}.[39−41] The relative intensity among these peaks is constant despite treatments in O_2, 2-propanol, or Ar at 300 °C, and no other peaks appear, suggesting that TiO_2 bulk is not reduced. If SMSI occurs, one can hypothesize that only TiO_2 in the close proximity to Au NPs gets reduced to promote the migration of the TiO_2 support over the Au NPs. The signal intensity corresponding to TiO_2 bands decreases upon generation of carbon deposits because of the self-absorption phenomenon,[42] suggesting that those deposits build over the entire TiO_2 support, even away from the Au NPs.

To test whether the TiO_2 support migrates onto the Au NPs upon 2-propanol treatment despite the existence of carbonaceous species, electron energy loss spectroscopy (EELS) was performed on the treated Au/TiO_2 sample as shown in Figure 2d. A line scan starting in vacuum (1), going through an "anchored" Au NP and finishing in the support was performed (the orange arrow in Figure 2d (left) shows the direction of the line scan). The section of the line scan corresponding to the Au NP without contribution from the support (between 2 and 3) shows the presence of carbon on the Au NP, along with weak signals for O and Ti. The weak relative intensity of the signals for O and Ti prevent us from upholding these results as an unambiguous proof of migration of a TiO_x layer over the Au NP.

These results confirm the formation of carbon deposits on the Au NPs but do not disprove the occurrence of SMSI. Hence, it is interesting to explore via density functional theory (DFT) whether the deposition of carbonaceous species on Au NPs and the formation a TiO_x overlayer (SMSI) could be associated.

Before studying the interaction of the Au-carbon-TiO_x interface, we evaluated whether the generation of SMSI would be thermodynamically favorable in the Au/TiO_2 system. The free energy of formation (ΔG) of the SMSI structure (Ti_xO_y layer over Au slab) was calculated at different oxygen chemical potentials ($\Delta\mu_{O_2}$). As seen in Figure S7, $\Delta G < 0$ for the Ti_2O_3/Au SMSI structure when $\Delta\mu_{O_2} < 4.2$ eV, showing that it is thermodynamically favorable under certain conditions. However, it has been shown before that Pt and Pd form more readily a SMSI structure on TiO_2 than Au.[19]

After calculations suggested that SMSI in the Au/TiO_2 system is feasible under certain conditions, we investigated the stability of the interaction between carbon species and TiO_x/Au interfaces. In Figure 3, carbon adsorption on model Au and TiO_x surfaces are shown on pristine Au(111) (−4.93 eV, Figure 3a), on pristine TiO_2 (−4.40 eV, Figure 3b), over a reduced TiO_2 vacancy (−1.56 eV, Figure 3c), and on $Ti_2O_3(001)$ (−5.19 eV, Figure 3d). To model the interface between Au NP covered by reduced TiO_2, a Ti_2O_3 monolayer is placed over the Au surface (Figure 3e−h). On this Ti_2O_3/Au

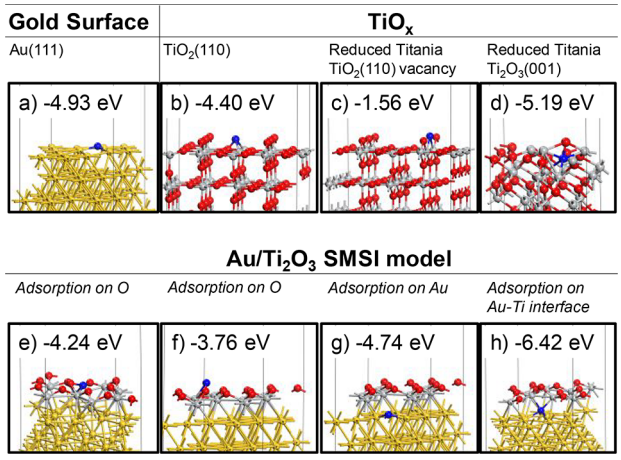

Figure 3. Adsorption energies for atomic carbon on various model systems: (a) Au(111), (b−d) TiO_x surfaces, (e−h) SMSI Au/Ti_2O_3. Adsorption energies are calculated with respect to atomic carbon in the gas phase. Color code: gold = yellow, carbon = blue, oxygen = red, titanium = gray.

SMSI model, we find that carbon can adsorb with similar strength atop the Ti_2O_3 layer (Figure 3e,f) and on the Au surface under the Ti_2O_3 layer (Figure 3g); interestingly, however, carbon adsorbs the strongest (−6.42 eV) when it is bound to both Au and Ti (Figure 3h). Despite the simplicity of the model, we find a strong indication that carbon−Ti−Au interactions would be thermodynamically feasible under the presence of SMSI. Furthermore, in a SMSI-like structure induced by 2-propanol, the migration of TiO_x to Au NPs could be further facilitated by the adsorbed carbon-containing species such as alkoxide. Such adsorbate-induced SMSI was also recently demonstrated by Matsubu et al.[12] and Liu et al.[18]

It is known that CO adsorption on the Au surface is rather weak compared to Pt-group metals. This is shown for CO adsorption on an O_2-300 °C treated Au/TiO_2 sample where the IR absorbance signal decreases quickly upon desorption in Ar at 30 °C (Figure 4a). Therefore, one could argue that the blockage induced by 2-propanol treatment may only occur at the perimeter Au−Ti sites, but the Au sites away from the support remain uncovered and nontitratable by CO due to extremely weak adsorption at 30 °C. To address this query, IR spectroscopy of CO adsorption at −143 °C on Au/TiO_2 was performed after 2-propanol treatment at 30 °C followed by Ar-flush at 300 °C (Figure 4b), and after reversing the overlayer by O_2 treatment at 300 °C (Figure 4c). After 2-propanol treatment at 30 °C and desorption at 300 °C in Ar, CO adsorption on Au is only a fraction (∼10%) (Figure 4b) of the adsorption when the sample is treated in O_2 at 300 °C (overlayer retreated, Figure 4c), supporting the formation of a blocking overlayer over the majority of the Au NPs after 2-propanol treatment, not just the perimeter sites. Treatment in 2-propanol generated, however, adsorption of CO on negatively charged $Au^{\delta-}$ with a characteristic band at 2075 cm^{-1} and also on Ti^{3+} species or surface oxygen vacancies with a vibrational mode at 2124−2127 cm^{-1} (Figure 4b), which supports at least partial reduction of the surface.[3,4,43] These $Au^{\delta-}$ adsorption sites are not evident in the fresh sample treated in O_2 at 300 °C (CO adsorption at 30 °C, Figure 4a) and the sample with a retracted overlayer (CO adsorption at −143 °C, Figure 4c). It has been previously reported that SMSI in the Au/TiO_2 system provokes electron donation from

https://dx.doi.org/10.1021/acscatal.0c02452
ACS Catal. 2020, 10, 8515−8523

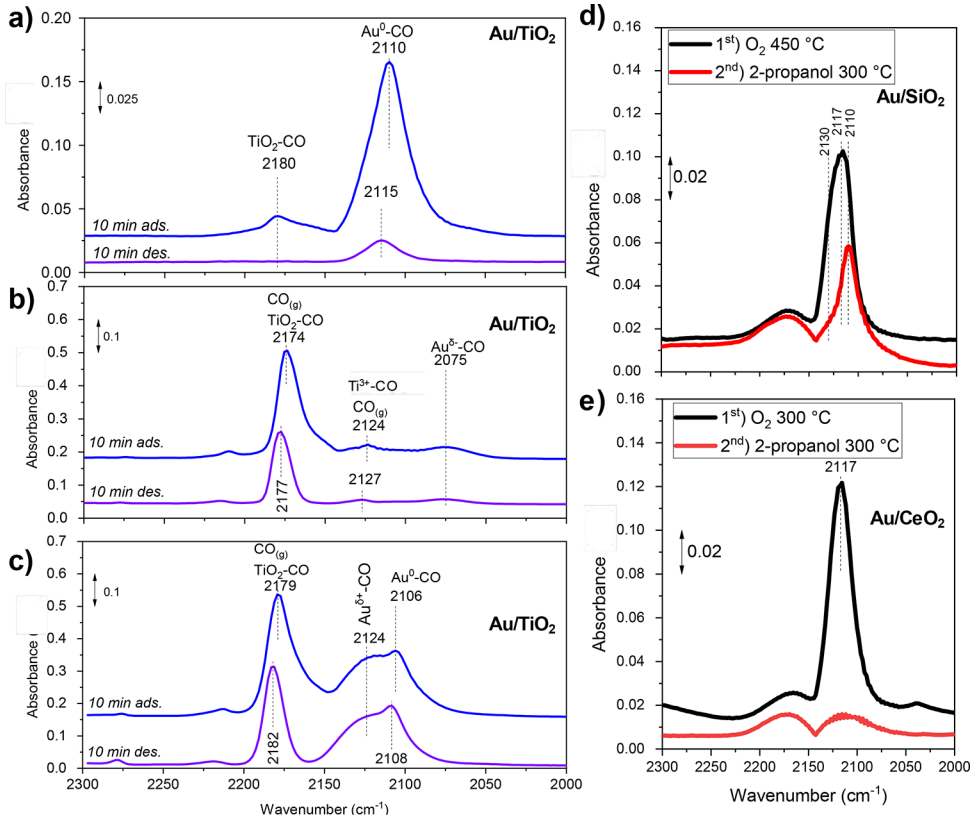

Figure 4. (a) FTIR spectroscopy of CO adsorption (10 min) and desorption (10 min) at 30 °C on Au/TiO_2 after treatment in O_2 at 300 °C. (b,c) FTIR spectroscopy of CO adsorption (10 min) and desorption (10 min) at −143 °C on Au/TiO_2: (b) after treatment in O_2 at 300 °C followed by treatment in 2-propanol at 30 °C (and postflush in Ar at 300 °C), (c) after treating the same sample load of b) in O_2 at 300 °C. (d,e) FTIR spectroscopy of CO adsorption (after 10 min) at 30 °C on (d) Au/SiO_2, and (e) Au/CeO_2 after treatment in O_2 at 300 or 450 °C, and treatment in 2-propanol at 300 °C (and postflush in Ar at 300 °C). Note: "1st", and "2nd" represent the sequence in the collection of spectra. Each "set" of spectra (there are four sets: panels a, b and c, d, and e) was collected for a fresh load catalyst in the DRIFTS cell.

the support to the Au NPs, thus generating an effective negative oxidation state on Au.[4] This evidence supports the creation of SMSI upon treatment in 2-propanol. CO adsorption on TiO_2 at −143 °C (Figure S8) was performed and confirmed the assignment of IR bands observed from CO adsorption on Au/TiO_2 in Figure 4b,c.

To test the hypothetical alcohol reduction-induced SMSI structure in Au/TiO_2, the availability of Au-sites was evaluated upon similar treatment of a nonreducible support, Au/SiO_2, and another reducible support, Au/CeO_2 (Figure 4d,e). On Au/SiO_2, fewer CO molecules adsorbed on Au-sites after 2-propanol treatment at 300 °C (and desorption in Ar at 300 °C), when compared with the base sample (treated in O_2), possibly due to residual carbonaceous species. Nonetheless, blockage of Au-sites was far from complete (Figure 4d). Au/CeO_2 did not present any IR band from adsorbed CO on Au NPs after 2-propanol treatment (Figure 4e), consistent with the picture that the occurrence of the SMSI-like coverage is accompanied by the reduction of the support. Nonetheless, we recognize that the comparison among Au/TiO_2, Au/SiO_2, and Au/CeO_2 is not completely conclusive. One could argue that Au/SiO_2 is simply less effective at activating 2-propanol to form adsorbates that would cover the actives sites, and therefore, the coverage of Au sites is not complete.[44]

At this stage, evidence shows the significant coverage of Au-site on reducible supports upon exposure to a common alcohol. It remains unclear whether strongly bound adsorbates, or SMSI, or both, are the reason for the observed blockage of Au-sites. Nevertheless, blockage of metal active sites via low-temperature treatment with an alcohol has important repercussions for studying the conversion of these alcohols over supported-metal catalysts. Since the catalytic oxidation of alcohols is a commonly studied system,[45−47] possible blockage of Au-sites was evaluated via IR spectroscopy after concurrent 2-propanol and O_2 treatment at 300 °C. IR of CO adsorption confirms the blockage of Au sites upon concurrent 2-propanol/O_2 (ratio 1:1.8) treatment (Figure S9). This suggests that the true active sites for alcohol conversion over supported Au NPs could be drastically different from what has been assumed previously (exposed Au sites) in the temperature range of ∼30−300 °C.[48−53]

Next, the implications of the blockage of Au-sites via 2-propanol treatment of Au/TiO_2 for catalytic oxidation of CO, chosen as a probe reaction, were studied. When CO oxidation was evaluated over Au/TiO_2 without any treatment in 2-propanol (no coverage of Au sites), monotonic deactivation with time-on-stream (TOS) was observed (Figure 5a), as has been previously reported.[3−6] When the sample was treated in 2-propanol at 300 °C, followed by treatment in O_2 at 200 °C, no catalytic activity for CO oxidation was observed ("O_2 200 °C" in Figure 5a), consistent with IR spectroscopy of CO adsorption, that showed no IR bands for adsorbed CO on Au (Figure 5b). To partially expose Au at the surface, thus making the Au-TiO_x interface available for CO oxidation, the blocking overlayer was retracted by increasing the temperature of the O_2-treatment (after treatment in 2-propanol at 300 °C). IR

https://dx.doi.org/10.1021/acscatal.0c02452
ACS Catal. 2020, 10, 8515−8523

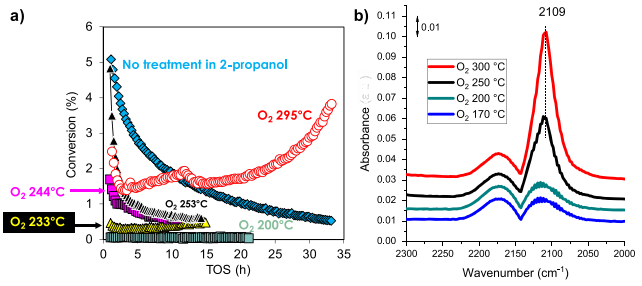

Figure 5. (a) Catalytic activity for CO oxidation at 50 °C (O_2/CO = 1.25) over Au/TiO_2. The run "O_2 200 °C" was performed after these pretreatments were performed: O_2 296 ± 2 °C, 4 h → 2-propanol 296 ± 2 °C, 2 h → O_2 200 °C, 2 h. The run labeled "No treatment in 2-propanol" was performed with 2.2 mg of catalyst, while other runs were performed with 42 mg. (b) FTIR spectroscopy of CO adsorption (after 10 min) at 30 °C. The two broad IR features at around 2120 and 2170 cm^{-1} are due to the gas-phase CO. Each spectrum was collected on a different load of the Au/TiO_2 catalyst. Each spectrum was collected after O_2 treatment following full coverage of Au NPs via 2-propanol treatment at 300 °C. For example, the spectrum "O_2 170 °C" was collected after these pretreatments were performed: O_2 300 °C, 30 min → 2-propanol 300 °C, 30 min → O_2 170 °C, 30 min.

spectroscopy of CO adsorption shows that O_2 treatment at a temperature between 200 and 250 °C enables the retraction of the overlayer blocking Au-sites, making CO adsorption possible. Increasing the O_2-treatment temperature, to further retract the blocking overlayer, from 250 to 300 °C, increased the amount of Au sites accessible to CO molecules, as evidenced by the intensity of the IR band at 2109 cm^{-1} (Figure 5b). In agreement with IR spectroscopy, catalytic results show that it is only when the oxidation treatment to retract the overlayer is performed at temperatures above 233 °C that catalytic activity is observed (Figure 5a).

CO oxidation over the sample with the blocking overlayer retracted, via O_2 treatment at 295 °C, showed an increase in rate with time-on-stream (TOS) after initial deactivation (Figure 5a). The production rate of CO_2 in Figure 5a ("O_2 295 °C") is correlated with a decrease in CO exiting the reactor, and thus, this CO_2 is not produced from the desorption of carbonaceous species deposited during treatment in 2-propanol (Figure S10). This increase in the rate of CO oxidation indicates that the density of catalytic sites increases with time-on-stream (TOS) and/or the catalytic sites become more active under reaction conditions. Although the fundamental reasons for this "self-activating" behavior warrant a future study, the induction of a blocking overlayer and the retraction of such layer provide a tuning knob for the catalysis of supported metal NPs.

CONCLUSIONS

Evidence suggests that common alcohols (2-propanol and methanol) can induce at least partial blockage of Au-sites in Au/TiO_2 at 30−300 °C. Exposure of Au/TiO_2 to 2-propanol at 30 °C, followed by desorption in Ar at 150 °C, induces the coverage of more than 95% of Au sites, unprecedented lower temperatures than those for traditional SMSI formation under H_2. Focused study of the treatment in 2-propanol showed that this blockage of Au-sites takes place for reducible oxides (Au/TiO_2, Au/CeO_2) but occurs to a much lesser extent in nonreducible oxides (Au/SiO_2), which is consistent with the occurrence of SMSI. However, it is reasonable to argue that Au/SiO_2 is not as effective at activating 2-propanol, thus generating less carbon deposits and less coverage of Au-sites. In conclusion, near-complete blockage of Au-sites upon exposure of reducible supports to a common alcohol at low temperatures has been demonstrated; however, it remains unclear whether this blockage is associated with carbon deposits, SMSI, or both.

Partial retraction of the blocking overlayer leads to self-activating catalytic sites in Au/TiO_2 for CO oxidation, whereas the catalyst without treatment in 2-propanol monotonically deactivates with TOS. The significance of this work is 2-fold: it is shown that modulating the degree of coverage of active sites through exposure to a common alcohol can lead to a new type of catalytic sites that may not be possible from other routes; the results also suggest that a common catalytic system such as the conversion of an alcohol over a supported-metal catalyst can induce *in situ* coverage of the active metal surface through carbon deposits and/or SMSI and thus calls for a reconsideration of the related reaction mechanism.

ASSOCIATED CONTENT

Supporting Information

The Supporting Information is available free of charge at https://pubs.acs.org/doi/10.1021/acscatal.0c02452.

XRD patterns, FTIR spectroscopy, TEM images, catalytic activity data, particle size distribution, evolution of species in the DRIFTS cell with treatment time, DFT calculations, and additional references (PDF)

AUTHOR INFORMATION

Corresponding Authors

Felipe Polo-Garzon − *Chemical Sciences Division, Oak Ridge National Laboratory, Oak Ridge, Tennessee 37831, United States;* orcid.org/0000-0002-6507-6183; Email: pologarzonf@ornl.gov

Zili Wu − *Chemical Sciences Division and Center for Nanophase Materials Sciences, Oak Ridge National Laboratory, Oak Ridge, Tennessee 37831, United States;* orcid.org/0000-0002-4468-3240; Email: wuz1@ornl.gov

Authors

Thomas F. Blum − *Center for Nanophase Materials Sciences, Oak Ridge National Laboratory, Oak Ridge, Tennessee 37831, United States*

Victor Fung − *Center for Nanophase Materials Sciences, Oak Ridge National Laboratory, Oak Ridge, Tennessee 37831, United States;* orcid.org/0000-0002-3347-6983

Zhenghong Bao − *Chemical Sciences Division, Oak Ridge National Laboratory, Oak Ridge, Tennessee 37831, United States*

Hao Chen − *Department of Chemistry, The University of Tennessee, Knoxville, Tennessee 37996, United States;* orcid.org/0000-0002-6658-4198

Zhennan Huang − *Center for Nanophase Materials Sciences, Oak Ridge National Laboratory, Oak Ridge, Tennessee 37831, United States*

Shannon M. Mahurin − *Chemical Sciences Division, Oak Ridge National Laboratory, Oak Ridge, Tennessee 37831, United States;* orcid.org/0000-0003-3792-1631

Sheng Dai − *Chemical Sciences Division, Oak Ridge National Laboratory, Oak Ridge, Tennessee 37831, United States; Department of Chemistry, The University of Tennessee,*

https://dx.doi.org/10.1021/acscatal.0c02452
ACS Catal. 2020, 10, 8515−8523

Knoxville, Tennessee 37996, United States; orcid.org/0000-0002-8046-3931

Miaofang Chi − *Center for Nanophase Materials Sciences, Oak Ridge National Laboratory, Oak Ridge, Tennessee 37831, United States;* orcid.org/0000-0003-0764-1567

Complete contact information is available at: https://pubs.acs.org/10.1021/acscatal.0c02452

Notes

This manuscript has been authored by UT-Battelle, LLC under Contract No. DE-AC05−00OR22725 with the U.S. Department of Energy. The United States Government retains and the publisher, by accepting the article for publication, acknowledges that the United States Government retains a nonexclusive, paid-up, irrevocable, worldwide license to publish or reproduce the published form of this manuscript, or allow others to do so, for United States Government purposes. The Department of Energy will provide public access to these results of federally sponsored research in accordance with the DOE Public Access Plan (http://energy.gov/downloads/doe-public-access-plan).

The authors declare no competing financial interest.

■ ACKNOWLEDGMENTS

This research is sponsored by the U.S. Department of Energy, Office of Science, Office of Basic Energy Sciences, Chemical Sciences, Geosciences, and Biosciences Division, Catalysis Science Program. Part of the work including IR, kinetic measurement and electron microscopy was conducted at the Center for Nanophase Materials Sciences, which is a DOE Office of Science User Facility. This research used resources of the National Energy Research Scientific Computing Center, a DOE Office of Science User Facility.

■ REFERENCES

(1) Ciriminna, R.; Falletta, E.; Della Pina, C.; Teles, J. H.; Pagliaro, M. Industrial Applications of Gold Catalysis. *Angew. Chem., Int. Ed.* **2016**, *55* (46), 14210−14217.

(2) Wrasman, C. J.; Boubnov, A.; Riscoe, A. R.; Hoffman, A. S.; Bare, S. R.; Cargnello, M. Synthesis of Colloidal Pd/Au Dilute Alloy Nanocrystals and Their Potential for Selective Catalytic Oxidations. *J. Am. Chem. Soc.* **2018**, *140* (40), 12930−12939.

(3) Zhang, J.; Wang, H.; Wang, L.; Ali, S.; Wang, C.; Wang, L.; Meng, X.; Li, B.; Su, D. S.; Xiao, F.-S. Wet-Chemistry Strong Metal−Support Interactions in Titania-Supported Au Catalysts. *J. Am. Chem. Soc.* **2019**, *141* (7), 2975−2983.

(4) Tang, H.; Su, Y.; Zhang, B.; Lee, A. F.; Isaacs, M. A.; Wilson, K.; Li, L.; Ren, Y.; Huang, J.; Haruta, M.; Qiao, B.; Liu, X.; Jin, C.; Su, D.; Wang, J.; Zhang, T. Classical strong metal−support interactions between gold nanoparticles and titanium dioxide. *Science Advances* **2017**, *3* (10), No. e1700231.

(5) Saavedra, J.; Doan, H. A.; Pursell, C. J.; Grabow, L. C.; Chandler, B. D. The critical role of water at the gold-titania interface in catalytic CO oxidation. *Science* **2014**, *345* (6204), 1599−1602.

(6) Konova, P.; Naydenov, A.; Venkov, C.; Mehandjiev, D.; Andreeva, D.; Tabakova, T. Activity and deactivation of Au/TiO2 catalyst in CO oxidation. *J. Mol. Catal. A: Chem.* **2004**, *213* (2), 235−240.

(7) Nijhuis, T. A.; Visser, T.; Weckhuysen, B. M. Mechanistic Study into the Direct Epoxidation of Propene over Gold/Titania Catalysts. *J. Phys. Chem. B* **2005**, *109* (41), 19309−19319.

(8) Tauster, S. J.; Fung, S. C.; Garten, R. L. Strong metal-support interactions. Group 8 noble metals supported on titanium dioxide. *J. Am. Chem. Soc.* **1978**, *100* (1), 170−175.

(9) Tauster, S. J.; Fung, S. C.; Baker, R. T. K.; Horsley, J. A. Strong Interactions in Supported-Metal Catalysts. *Science* **1981**, *211* (4487), 1121−1125.

(10) Sá, J.; Bernardi, J.; Anderson, J. A. Imaging of low temperature induced SMSI on Pd/TiO2 catalysts. *Catal. Lett.* **2007**, *114* (1), 91−95.

(11) Sonström, P.; Arndt, D.; Wang, X.; Zielasek, V.; Bäumer, M. Ligand Capping of Colloidally Synthesized Nanoparticles—A Way to Tune Metal−Support Interactions in Heterogeneous Gas-Phase Catalysis. *Angew. Chem., Int. Ed.* **2011**, *50* (17), 3888−3891.

(12) Matsubu, J. C.; Zhang, S.; DeRita, L.; Marinkovic, N. S.; Chen, J. G.; Graham, G. W.; Pan, X.; Christopher, P. Adsorbate-mediated strong metal−support interactions in oxide-supported Rh catalysts. *Nat. Chem.* **2017**, *9*, 120.

(13) Caballero, A.; Holgado, J. P.; Gonzalez-Delacruz, V. M.; Habas, S. E.; Herranz, T.; Salmeron, M. In situ spectroscopic detection of SMSI effect in a Ni/CeO2 system: hydrogen-induced burial and dig out of metallic nickel. *Chem. Commun.* **2010**, *46* (7), 1097−1099.

(14) Shi, X. Y.; Zhang, W.; Zhang, C.; Zheng, W. T.; Chen, H.; Qi, J. G. Real-space observation of strong metal-support interaction: state-of-the-art and what's the next. *J. Microsc.* **2016**, *262* (3), 203−215.

(15) Ro, I.; Resasco, J.; Christopher, P. Approaches for Understanding and Controlling Interfacial Effects in Oxide-Supported Metal Catalysts. *ACS Catal.* **2018**, *8* (8), 7368−7387.

(16) Tang, H.; Wei, J.; Liu, F.; Qiao, B.; Pan, X.; Li, L.; Liu, J.; Wang, J.; Zhang, T. Strong Metal−Support Interactions between Gold Nanoparticles and Nonoxides. *J. Am. Chem. Soc.* **2016**, *138* (1), 56−59.

(17) Tang, H.; Liu, F.; Wei, J.; Qiao, B.; Zhao, K.; Su, Y.; Jin, C.; Li, L.; Liu, J.; Wang, J.; Zhang, T. Ultrastable Hydroxyapatite/Titanium-Dioxide-Supported Gold Nanocatalyst with Strong Metal−Support Interaction for Carbon Monoxide Oxidation. *Angew. Chem., Int. Ed.* **2016**, *55* (36), 10606−10611.

(18) Liu, S.; Xu, W.; Niu, Y.; Zhang, B.; Zheng, L.; Liu, W.; Li, L.; Wang, J. Ultrastable Au nanoparticles on titania through an encapsulation strategy under oxidative atmosphere. *Nat. Commun.* **2019**, *10* (1), 5790.

(19) Zhang, S.; Plessow, P. N.; Willis, J. J.; Dai, S.; Xu, M.; Graham, G. W.; Cargnello, M.; Abild-Pedersen, F.; Pan, X. Dynamical Observation and Detailed Description of Catalysts under Strong Metal−Support Interaction. *Nano Lett.* **2016**, *16* (7), 4528−4534.

(20) Gao, Y.; Liang, Y.; Chambers, S. A. Thermal stability and the role of oxygen vacancy defects in strong metal support interaction — Pt on Nb-doped TiO2(100). *Surf. Sci.* **1996**, *365* (3), 638−648.

(21) Fu, Q.; Wagner, T.; Olliges, S.; Carstanjen, H.-D. Metal-Oxide Interfacial Reactions: Encapsulation of Pd on TiO2 (110). *J. Phys. Chem. B* **2005**, *109* (2), 944−951.

(22) Mullins, D. R.; Robbins, M. D.; Zhou, J. Adsorption and reaction of methanol on thin-film cerium oxide. *Surf. Sci.* **2006**, *600* (7), 1547−1558.

(23) Sutton, J. E.; Overbury, S. H.; Beste, A. Coadsorbed Species Explain the Mechanism of Methanol Temperature-Programmed Desorption on CeO2(111). *J. Phys. Chem. C* **2016**, *120* (13), 7241−7247.

(24) Kim, K. S.; Barteau, M. A.; Farneth, W. E. Adsorption and decomposition of aliphatic alcohols on titania. *Langmuir* **1988**, *4* (3), 533−543.

(25) Argyle, M. D. B. C.H.; Bartholomew, C. Heterogeneous Catalyst Deactivation and Regeneration: A Review. *Catalysts* **2015**, *5* (1), 145−269.

(26) Wu, Z.; Jiang, D.-E.; Mann, A. K. P.; Mullins, D. R.; Qiao, Z.-A.; Allard, L. F.; Zeng, C.; Jin, R.; Overbury, S. H. Thiolate Ligands as a Double-Edged Sword for CO Oxidation on CeO_2 Supported Au25(SCH2CH2Ph)18 Nanoclusters. *J. Am. Chem. Soc.* **2014**, *136* (16), 6111−6122.

(27) Long, C. G.; Gilbertson, J. D.; Vijayaraghavan, G.; Stevenson, K. J.; Pursell, C. J.; Chandler, B. D. Kinetic Evaluation of Highly Active Supported Gold Catalysts Prepared from Monolayer-Protected Clusters: An Experimental Michaelis-Menten Approach for Determin-

ing the Oxygen Binding Constant during CO Oxidation Catalysis. *J. Am. Chem. Soc.* **2008**, *130* (31), 10103−10115.
(28) Zhu, H.; Liang, C.; Yan, W.; Overbury, S. H.; Dai, S. Preparation of Highly Active Silica-Supported Au Catalysts for CO Oxidation by a Solution-Based Technique. *J. Phys. Chem. B* **2006**, *110* (22), 10842−10848.
(29) Mai, H.-X.; Sun, L.-D.; Zhang, Y.-W.; Si, R.; Feng, W.; Zhang, H.-P.; Liu, H.-C.; Yan, C.-H. Shape-Selective Synthesis and Oxygen Storage Behavior of Ceria Nanopolyhedra, Nanorods, and Nanocubes. *J. Phys. Chem. B* **2005**, *109* (51), 24380−24385.
(30) Brunauer, S.; Emmett, P. H.; Teller, E. Adsorption of Gases in Multimolecular Layers. *J. Am. Chem. Soc.* **1938**, *60* (2), 309−319.
(31) Wu, Z.; Li, M.; Howe, J.; Meyer, H. M.; Overbury, S. H. Probing Defect Sites on CeO2 Nanocrystals with Well-Defined Surface Planes by Raman Spectroscopy and O2 Adsorption. *Langmuir* **2010**, *26* (21), 16595−16606.
(32) Kresse, G.; Furthmüller, J. Efficiency of ab-initio total energy calculations for metals and semiconductors using a plane-wave basis set. *Comput. Mater. Sci.* **1996**, *6* (1), 15−50.
(33) Kresse, G.; Furthmuller, J. Efficient iterative schemes for ab initio total-energy calculations using a plane-wave basis set. *Phys. Rev. B: Condens. Matter Mater. Phys.* **1996**, *54* (16), 11169−11186.
(34) Perdew, J. P.; Burke, K.; Ernzerhof, M. Generalized Gradient Approximation Made Simple. *Phys. Rev. Lett.* **1996**, *77* (18), 3865−3868.
(35) Kresse, G.; Joubert, D. From ultrasoft pseudopotentials to the projector augmented-wave method. *Phys. Rev. B: Condens. Matter Mater. Phys.* **1999**, *59* (3), 1758−1775.
(36) Blochl, P. E. Projector Augmented-Wave Method. *Phys. Rev. B: Condens. Matter Mater. Phys.* **1994**, *50* (24), 17953−17979.
(37) Green, I. X.; Tang, W.; Neurock, M.; Yates, J. T. Spectroscopic Observation of Dual Catalytic Sites During Oxidation of CO on a Au/TiO_2 Catalyst. *Science* **2011**, *333* (6043), 736−739.
(38) Panayotov, D. A.; Burrows, S. P.; Yates, J. T.; Morris, J. R. Mechanistic Studies of Hydrogen Dissociation and Spillover on Au/TiO2: IR Spectroscopy of Coadsorbed CO and H-Donated Electrons. *J. Phys. Chem. C* **2011**, *115* (45), 22400−22408.
(39) Rodríguez, L. A. A.; Pianassola, M.; Travessa, D. N. Production of TiO2 Coated Multiwall Carbon Nanotubes by the Sol-Gel Technique. *Mater. Res.* **2017**, *20*, 96−103.
(40) Gui, M. M.; Chai, S.-P.; Xu, B.-Q.; Mohamed, A. R. Visible-light-driven MWCNT@TiO2 core−shell nanocomposites and the roles of MWCNTs on the surface chemistry, optical properties and reactivity in CO2 photoreduction. *RSC Adv.* **2014**, *4* (46), 24007−24013.
(41) Hamid, S. B. A.; Tan, T. L.; Lai, C. W.; Samsudin, E. M. Multiwalled carbon nanotube/TiO2 nanocomposite as a highly active photocatalyst for photodegradation of Reactive Black 5 dye. *Chinese Journal of Catalysis* **2014**, *35* (12), 2014−2019.
(42) Wu, Z.; Zhang, C.; Stair, P. C. Influence of absorption on quantitative analysis in Raman spectroscopy. *Catal. Today* **2006**, *113* (1), 40−47.
(43) Liao, L. F.; Lien, C. F.; Shieh, D. L.; Chen, M. T.; Lin, J. L. FTIR Study of Adsorption and Photoassisted Oxygen Isotopic Exchange of Carbon Monoxide, Carbon Dioxide, Carbonate, and Formate on TiO2. *J. Phys. Chem. B* **2002**, *106* (43), 11240−11245.
(44) Wu, Y. Y.; Kung, H. H. Probing properties of the interfacial perimeter sites in TiOx/Au/SiO2 with 2-propanol decomposition. *Appl. Catal., A* **2017**, *548*, 150−163.
(45) Mallat, T.; Baiker, A. Oxidation of Alcohols with Molecular Oxygen on Solid Catalysts. *Chem. Rev.* **2004**, *104* (6), 3037−3058.
(46) Parmeggiani, C.; Matassini, C.; Cardona, F. A step forward towards sustainable aerobic alcohol oxidation: new and revised catalysts based on transition metals on solid supports. *Green Chem.* **2017**, *19* (9), 2030−2050.
(47) Ali, M. E.; Rahman, M. M.; Sarkar, S. M.; Hamid, S. B. A. Heterogeneous metal catalysts for oxidation reactions. *J. Nanomater.* **2014**, *2014*, 192038.
(48) Farnesi Camellone, M.; Zhao, J.; Jin, L.; Wang, Y.; Muhler, M.; Marx, D. Molecular Understanding of Reactivity and Selectivity for Methanol Oxidation at the Au/TiO2 Interface. *Angew. Chem., Int. Ed.* **2013**, *52* (22), 5780−5784.
(49) Abad, A.; Concepción, P.; Corma, A.; García, H. A Collaborative Effect between Gold and a Support Induces the Selective Oxidation of Alcohols. *Angew. Chem., Int. Ed.* **2005**, *44* (26), 4066−4069.
(50) Abad, A.; Corma, A.; García, H. Catalyst Parameters Determining Activity and Selectivity of Supported Gold Nanoparticles for the Aerobic Oxidation of Alcohols: The Molecular Reaction Mechanism. *Chem. - Eur. J.* **2008**, *14* (1), 212−222.
(51) Sudarsanam, P.; Mallesham, B.; Durgasri, D. N.; Reddy, B. M. Physicochemical and catalytic properties of nanosized Au/CeO2 catalysts for eco-friendly oxidation of benzyl alcohol. *J. Ind. Eng. Chem.* **2014**, *20* (5), 3115−3121.
(52) Holz, M. C.; Kähler, K.; Tölle, K.; van Veen, A. C.; Muhler, M. Gas-phase oxidation of 2-propanol over Au/TiO2 catalysts to probe metal−support interactions. *Phys. Status Solidi B* **2013**, *250* (6), 1094−1106.
(53) Heeskens, D.; Aghaei, P.; Kaluza, S.; Strunk, J.; Muhler, M. Selective oxidation of ethanol in the liquid phase over Au/TiO2. *Phys. Status Solidi B* **2013**, *250* (6), 1107−1118.

NOTE ADDED AFTER ASAP PUBLICATION

This paper was originally published ASAP on July 20, 2020. Due to a production error, a correction was missed in the equation of the DFT Calculations section. The revised version was reposted on July 20, 2020.

https://dx.doi.org/10.1021/acscatal.0c02452
ACS Catal. 2020, 10, 8515−8523